Response of jammed packings to thermal fluctuations

Qikai Wu, Thibault Bertrand, Mark D. Shattuck, and Corey S. O'Hern

Phys. Rev. E **96**, 062902 — Published 1 December 2017

DOI: 10.1103/PhysRevE.96.062902

The response of jammed packings to thermal fluctuations

Qikai Wu,[1] Thibault Bertrand,[2] Mark D. Shattuck,[3,1] and Corey S. O'Hern[1,4,5]

[1]*Department of Mechanical Engineering and Materials Science, Yale University, New Haven, Connecticut, 06520, USA*
[2]*Laboratoire Jean Perrin UMR 8237 CNRS/UPMC, Université Pierre et Marie Curie, 75255 Paris Cedex, France*
[3]*Department of Physics and Benjamin Levich Institute, The City College of the City University of New York, New York, 10031, USA*
[4]*Department of Physics, Yale University, New Haven, Connecticut, 06520, USA*
[5]*Department of Applied Physics, Yale University, New Haven, Connecticut, 06520, USA*

(Dated: November 20, 2017)

We focus on the response of mechanically stable (MS) packings of frictionless, bidisperse disks to thermal fluctuations, with the aim of quantifying how nonlinearities affect system properties at finite temperature. In contrast, numerous prior studies characterized the structural and mechanical properties of MS packings of frictionless spherical particles at *zero temperature*. Packings of disks with purely repulsive contact interactions possess two main types of nonlinearities, one from the form of the interaction potential (e.g. either linear or Hertzian spring interactions) and one from the breaking (or forming) of interparticle contacts. To identify the temperature regime at which the contact-breaking nonlinearities begin to contribute, we first calculated the minimum temperatures T_{cb} required to break a single contact in the MS packing for both single and multiple eigenmode perturbations of the $T = 0$ MS packing. We find that the temperature required to break a single contact for equal velocity-amplitude perturbations involving all eigenmodes approaches the minimum value obtained for a perturbation in the direction connecting disk pairs with the smallest overlap. We then studied deviations in the constant volume specific heat C_V and deviations of the average disk positions Δr from their $T = 0$ values in the temperature regime $T_{cb} < T < T_r$, where T_r is the temperature beyond which the system samples the basin of a new MS packing. We find that the deviation in the specific heat per particle $\Delta\overline{C}_V^0/\overline{C}_V^0$ relative to the zero temperature value $\overline{C}_V^0$ can grow rapidly above T_{cb}, however, the deviation $\Delta\overline{C}_V^0/\overline{C}_V^0$ decreases as N^{-1} with increasing system size. To characterize the relative strength of contact-breaking versus form nonlinearities, we measured the ratio of the average position deviations $\Delta r^{ss}/\Delta r^{ds}$ for single- and double-sided linear and nonlinear spring interactions. We find that $\Delta r^{ss}/\Delta r^{ds} > 100$ for linear spring interactions is independent of system size. This result emphasizes that contact-breaking nonlinearities are dominant over form nonlinearities in the low temperature range $T_{cb} < T < T_r$ for model jammed systems.

PACS numbers: 45.70.–n, 63.50.–x, 64.70.pv

I. INTRODUCTION

Static packings of frictionless disks and spheres are informative model systems for studying jamming in granular media [1] and dense colloidal suspensions [2]. Mechanically stable (MS) packings of frictionless disks in two spatial dimensions (2D) are isostatic at jamming onset [3] and possess $N_c^0 = 2N' - 1$ contacts (with periodic boundary conditions), where $N' = N - N_r$ is the number of disks in the force-bearing contact network, N is the total number of disks, and N_r is the number of "rattler" disks with fewer than three contacts per disk [4]. (See Fig. 1 (a) and (b).) Mechanically stable disk packings possess a full spectrum of $2N' - 2$ nonzero eigenvalues of the dynamical matrix (i.e. the Hessian of the interaction potential [5]), which represent the vibrational frequencies of the zero-temperature packings in the harmonic approximation. The structural and mechanical properties of isostatic disk and sphere packings near jamming at *zero temperature* have been reviewed extensively [6–8], including the pressure scaling of the bulk and shear moduli, excess contact number, and low-frequency plateau in the density of vibrational modes near jamming onset. More recently, several groups have investigated how the scaling behavior of these quantities is affected by thermal fluctuations using computer simulations [9–12], and mechanical vibrations in experiments of granular media [13–15].

Several authors have used computer simulations of soft disks that interact via purely repulsive linear spring potentials to study how the density of vibrational modes of mechanically stable packings at zero temperature and finite overcompression (with potential energy per particle $U > 0$) changes with increasing temperature. This work has shown that there is a characteristic temperature $T^* \sim U \sim \Delta\phi^2$, where $\Delta\phi = \phi - \phi_J$ is the deviation in the packing fraction above jamming onset at ϕ_J, above which the density of vibrational modes begins to deviate strongly from that at zero temperature [10, 11, 16]. In addition, they showed that T^* corresponds to the temperature above which an extensive number of the contacts in the $T = 0$ contact network has broken.

In prior publications [11, 17], we performed computational studies to measure the temperature at which linear response breaks down. This question is very important,

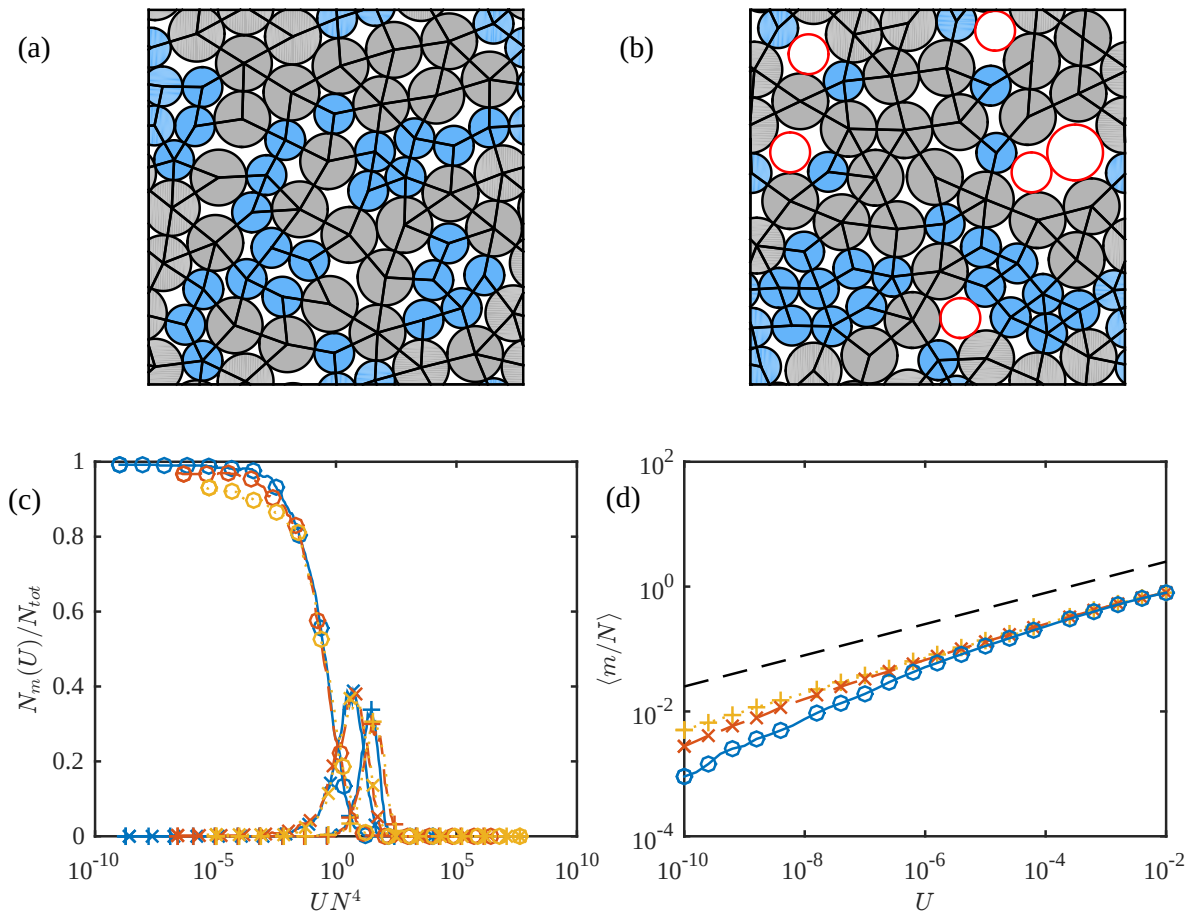

FIG. 1: Examples of isostatic mechanically stable bidisperse disk packings at zero temperature with (a) $N_c = N_c^0 = 127$ contacts and $N_r = 0$ rattler particles and (b) $N_c = N_c^0 = 115$ contacts and $N_r = 6$ rattler particles. The non-rattler (rattler) disks are outlined in black (red). For both (a) and (b), the total number of disks $N = 64$, the potential energy per particle $U = 10^{-12}$, and the solid black lines connecting disks centers indicate force-bearing interparticle contacts. (c) The fraction of mechanically stable packings $N_m(U)/N_{\rm tot}$ that possess $m = N_c - N_c^0 = 0$ (circles), 2 (exes), and 4 (plus signs) excess contacts as a function of UN^4 for three system sizes $N = 32$ (solid lines), 128 (dashed lines), and 256 (dotted lines). (d) The number of excess contacts m normalized by N averaged over 5000 MS packings and plotted versus U for three system sizes $N = 32$ (circles), 128 (exes), and 256 (plus signs). The dashed line has slope 0.25.

but also subtle, since one can define linear response in a strict sense (in which the particle positions and velocities oscillate at frequencies given by the eigenfrequencies of the dynamical matrix) or in a less strict sense (in which the binned density of states is similar to that at zero temperature). It is known that both contact breaking and nonlinearities from the form of the interparticle potential can contribute to the breakdown of linear response. However, the relative strengths of the nonlinearities arising from these two effects have not been measured for packings of purely repulsive frictionless particles. The present work contributes to the understanding of the breakdown of linear response by measuring the relative strength of the contact breaking nonlinearities and nonlinearities from the form of the interparticle potential at temperatures near and above the first contact breaking, and below the temperature at which particle rearrangements occur.

As mentioned above, an extensive number of broken contacts (or more [12]) are required to significantly change the binned density of vibrational modes. However, do any important physical quantities change when a single contact or sub-extensive number of contacts in the zero-temperature contact network is broken by thermal fluctuations? The answer to this question may depend on the number of excess contacts in the $T = 0$ contact network $m = N_c - N_c^0$. For example, if a zero-temperature packing has zero excess contacts ($m = 0$), the breaking of a single contact would cause the system to become unjammed. In Fig. 1 (c), we show the fraction of MS packings with m excess contacts, $N_m(U)/N_{tot}$, can be collapsed for each m and different system sizes by plotting $N_m(U)/N_{tot}$ as a function of UN^4. We find that the average number of excess contacts scales as $\langle m \rangle / N \sim U^{1/4}$ (Fig. 1 (d)), which is consistent with previous studies at zero temperature [6]. Thus, in the large-system limit

isostatic packings with $m = 0$ exist only at $U = 0$.

In this article, we will first characterize the minimum temperature required to break a single contact as a function of the protocol used to add thermal fluctuations. We focus on this quantity because it can be determined exactly in the low-temperature limit from the eigenvalues and eigenmodes of the dynamical matrix for the $T = 0$ MS packings. In particular, we will measure the minimum temperature $T_1(m, m-1)$ above which a $T = 0$ MS packing with m excess contacts changes to a packing with $m-1$ excess contacts in response to a perturbation along a single eigenmode. Thermal fluctuations can also be added to the zero-temperature MS packing by perturbing the system along a superposition of n eigenmodes of the dynamical matrix, and we can measure the minimum temperature, $T_n(m, m-1)$, required to break a single contact. We will show that that the minimum temperature required to break a single contact over all single mode excitations scales as $T_1(m, m-1) \sim U/N^{\alpha}$, where $\alpha \approx 2.6 \pm 0.1$, which is consistent with previous measurements [17]. For multi-mode excitations, $T_n(m, m-1)$ decreases as the number of eigenmodes n involved in the perturbation increases, reaching a minimum for perturbations with equipartition of all $2N'$ eigenmodes. The minimum temperature required to break a single contact for a perturbation with equipartition of all eigenmodes of the $T = 0$ dynamical matrix scales as $T_{2N'}(m, m-1) \sim N^{-\beta}$, where $\beta \approx 2.9 \pm 0.1$. This system-size size dependence is stronger than that for single-mode perturbations.

We also measured the temperature required to break multiple contacts. In this case, we employed molecular dynamics simulations to determine the temperature at which a given fraction of simulation snapshots possess a specified number of contacts. This information cannot be obtained from the $T = 0$ dynamical matrix, since the eigenmodes change after contacts begin breaking. We find a power-law scaling relation between the temperature, number of broken contacts $N_{bc} = N_c^0 + m - N_c$, system size, and potential energy per particle U.

After investigating the temperatures at which a given number of zero-temperature contacts break, we search for physical quantities that may be sensitive to small changes in the interparticle contact networks. We focused on two quantities: 1) the deviation in the specific heat $\Delta C_V/C_V^0 = (C_V - C_V^0)/C_V^0$ from the zero temperature value C_V^0 and 2) the deviation of the average positions of the disks $\overline{x}_i$ and $\overline{y}_i$ in a packing at a given temperature, $\Delta r = \sqrt{\sum_{i=1}^{N}[(\bar{x}_i - x_i^0)^2 + (\bar{y}_i - y_i^0)^2]/N}$, from the $T = 0$ disk positions, $\vec{R}^0 = \{x_1^0, y_1^0, \ldots, x_{N'}^0, y_{N'}^0\}$. Calculating Δr is important for understanding how far the initial packing can move in configuration space before transitioning to the basin of a new MS packing. We compare Δr^{ss} for systems with purely repulsive (single-sided) linear and nonlinear spring interactions to Δr^{ds} obtained for systems with double-sided linear and nonlinear spring interactions, which allows us to quantify the additional nonlinearities that arise from contact breaking. We find that both quantities, $\Delta C_V/C_V^0$ and $\Delta r^{ss}/\Delta r^{ds}$ are sensitive to the breaking of a *single contact*. However, the deviation $\Delta C_V/C_V^0$ decreases with increasing system size. In contrast, $\Delta r^{ss}/\Delta r^{ds} > 100$ for purely repulsive linear springs and does not depend strongly on system size. We also quantify $\Delta r^{ss}/\Delta r^{ds}$ for packings with Hertzian spring interactions and show that contact breaking increases the magnitude of the nonlinearities at finite temperature, but not as much as for linear repulsive spring interactions.

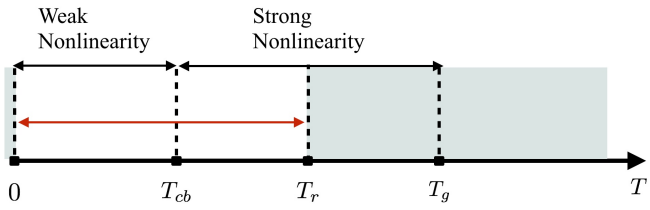

FIG. 2: Schematic of four important temperature regimes when studying the response of MS packings to thermal fluctuations. For $T < T_{cb}$, the $T = 0$ contact network remains intact. In this regime, "form" nonlinearities occur when the interparticle potential cannot be written exactly as a harmonic function of the disk positions. For $T_{cb} < T < T_r$, the $T = 0$ contact network changes, both form and contact-breaking nonlinearities occur, and the system remains in the basin of attraction of the original MS packing. For $T_r < T < T_g$, the system can move to the basins of attraction of other MS packings, but the relaxation times are sufficiently long that structural relaxation is not complete. For $T > T_g$, the system is liquid-like with finite structural relaxation times. This article focuses on the (unshaded) temperature regimes that occur for $0 < T \leq T_r$.

There are several important temperature scales to consider when studying the response of MS packings to thermal fluctuations. In Fig. 2, we show four temperature regimes: $0 < T < T_{cb}$, $T_{cb} < T < T_r$, $T_r < T < T_g$, and $T > T_g$. For $0 < T < T_{cb}$, where T_{cb} is the minimum temperature at which a single contact breaks, the system is weakly nonlinear with "form" nonlinearities that arise when the interaction potential cannot be expressed exactly as a harmonic function of the disk positions. (We use the notation T_{cb} for the temperature required to break a single contact when we do not specify the type of initial perturbation.) In the temperature regime $T_{cb} < T < T_r$, contacts begin breaking, both form and contact-breaking nonlinearities occur, and the system remains in the basin of attraction of the original MS packing. In this regime Δr^{ss} can be much larger than Δr^{ds} due to contact-breaking nonlinearities. At larger temperatures, $T_r < T < T_g$, the system rearranges and moves beyond the basin of attraction of the original $T = 0$ MS packing, but the timescales are prohibitively long to allow complete structural relaxation. Finally for $T > T_g$, the system is liquid-like with a finite structural relaxation time.

We emphasize that a number of studies have char-

acterized the structural and mechanical properties of MS packings at $T = 0$ [18–20]. Further, many studies have tracked the growth of the dynamical heterogeneities and the structural relaxation times as $T \to T_g$ from above [21–23]. However, few studies have focused on the low-temperature regimes $0 < T < T_{cb}$ and $T_{cb} < T < T_r$, where the contribution of contact breaking to the magnitude of the nonlinearities can be quantified at finite temperature. In future work, we will focus on the temperature regime $T_r < T < T_g$ to understand the connection between the geometry of the high-dimensional energy landscape and slow structural relaxation.

The remainder of this article will be organized as follows. In Sec. II, we describe the methods we employ to generate zero-temperature MS packings, the protocols used to add thermal fluctuations to the MS packings, and the measurements of the changes in the specific heat $\Delta C_V^0/C_V^0$ and average particle positions Δr of the packings from their $T = 0$ values as a function of temperature. In Sec. III, we present our results for $\Delta C_V/C_V^0$ and Δr. We show that $\Delta C_V/C_V^0$ increases more strongly when a single contact in the $T = 0$ MS packing changes. We find that $\Delta C_V/C_V^0$ decreases with increasing system size, however, the quantity $\Delta r^{ss}/\Delta r^{ds}$, which identifies the distinct contribution of contact breaking to the nonlinear response, does not depend strongly on system size. In Sec. IV, we summarize our results and highlight promising future research directions that stem from this work. We also provide several Appendices that include additional details of the methods and calculations we implement. In Appendix A, we provide additional details concerning the method we used to calculate the minimum temperature required to break a single contact with perturbations that involve n eigenmodes of the $T = 0$ dynamical matrix with equal velocity amplitudes. In Appendix B, we discuss the additional nonlinearities that arise from rattlers in MS packings and affect $\Delta r(T)$ at finite temperatures. In Appendix C, we describe the methods that we employed to measure the rearrangement T_r and glass transition T_g temperatures. Finally, in Appendix D, we show that the leading order term in the change in the average position scales linearly with temperature, $\Delta r \sim T$, for a particle in a one-dimensional cubic potential well.

II. METHODS

Our computational studies focus on measuring the response of MS packings composed of N bidisperse frictionless disks ($N/2$ large and $N/2$ small disks with diameter ratio $\sigma_L/\sigma_S = 1.4$) to thermal fluctuations with system sizes in the range from $N = 16$ to 1024 disks using periodic boundaries in square simulation cells. The disks (all with mass m) interact via the pairwise, purely repulsive potential,

$$U(r_{ij}) = \frac{\epsilon}{\alpha}\left(1 - \frac{r_{ij}}{\sigma_{ij}}\right)^{\alpha} \Theta\left(1 - \frac{r_{ij}}{\sigma_{ij}}\right), \qquad (1)$$

where r_{ij} is the separation between the centers of disks i and j, $\sigma_{ij} = (\sigma_i + \sigma_j)/2$ is the average disk diameter, ϵ is the energy scale of the repulsive interaction, $\Theta(x)$ is the Heaviside step function, and $\alpha = 2$ (5/2) corresponds to linear (Hertzian) repulsive spring interactions. We also consider disk packings that interact via double-sided spring potentials with a similar form to that in Eq. 1:

$$U_{ds}(r_{ij}) = \frac{\epsilon}{\alpha}\left|1 - \frac{r_{ij}}{\sigma_{ij}}\right|^{\alpha}. \qquad (2)$$

For studies involving interactions in Eq. 2, the interparticle contact network is fixed to that in the $T = 0$ MS packing for all temperatures [24]. Comparison of the results from single- versus double-sided interactions allows us to determine the strength of the nonlinearities that arise from contact breaking alone.

We generate MS packings as function of the total potential energy per particle $U = \Sigma_{i>j}U(r_{ij})/N$ using a protocol that successively compresses or decompresses the system in small packing fraction steps $\Delta\phi$ followed by conjugate gradient energy minimization [4]. The compression/decompression protocol is terminated when the total potential energy per particle satisfies $|U_c - U|/U < 10^{-16}$, where U_c is the current and U is the target potential energy per particle.

Another type of packing generation protocol could involve cooling to a nonzero temperature $T > 0$ of interest. If the cooling rate is too slow or the final temperature of the packing is too high, particle rearrangements can occur. We have shown in previous studies that such protocols give rise to microphase separation and local ordering in bidisperse systems [25]. In contrast, here we focus on fast quenches and packings with final temperatures $T < T_r$ below the temperature required to induce particle rearrangements. Thus, cooling to zero temperature and then heating up to a finite temperature T will yield the same results as generating a packing directly at a nonzero temperature.

The initial perturbations will be applied along one or more of the eigenmodes of the dynamical matrix of the $T = 0$ MS packings. We denote the $2N' - 2$ non-zero eigenfrequencies of the dynamical matrix as $\{\omega^1, \ldots, \omega^{2N'-2}\}$. Each eigenfrequency ω^i has an associated eigenvector $\hat{E}^i = \{e^i_{x1}, e^i_{y1}, e^i_{x2}, e^i_{y2}, \ldots, e^i_{xN'}, e^i_{yN'}\}$ that satisfies $(\hat{E}^i)^2 = 1$. The disk velocities $\vec{V}^0 = \{v^0_{x1}, v^0_{y1}, \ldots, v^0_{xN'}, v^0_{xN'}\}$ corresponding to the initial perturbation can be expressed as a linear combination of the eigenmodes of the dynamical matrix:

$$\vec{V}^0 = \sum_{i=1}^{2N'-2} A_i \omega^i \hat{E}^i. \qquad (3)$$

We will use the notation that upper case vectors, e.g. $\vec{R}$ and $\vec{V}$, include both the particle and spatial dimensions, while lower case vectors, e.g. $\vec{r}$ and $\vec{v}$, only include the spatial dimensions.

For sufficiently small amplitude perturbations, the time evolution of the multi-particle velocities and positions are given in the harmonic approximation by

$$\vec{V}(t) = \sum_{i=1}^{2N'-2} A_i \omega^i \hat{E}^i \cos(\omega^i t), \tag{4}$$

and

$$\vec{R}(t) = \vec{R}^0 + \sum_{i=1}^{2N'-2} A_i \hat{E}^i \sin(\omega^i t), \tag{5}$$

where $\vec{R}^0$ gives the disk positions in the $T = 0$ MS packing. We calculate the temperature of the system using the average kinetic energy per particle K/N [26].

For sufficiently large temperatures, when multiple $T = 0$ contacts break and new contacts form, we cannot use the $T = 0$ eigenmodes of the dynamical matrix to determine the properties of the contact networks. Thus, we will characterize the relation between the temperature, number of contacts, system size, and potential energy per particle using molecular dynamics simulations at constant number of disks, area, and total energy E. For the MD simulations, we use the velocity Verlet integration scheme with a time step $\Delta t \sim t_{\rm col}/40$, where $t_{\rm col} = \sigma_S\sqrt{\epsilon/m}$ is a typical interparticle collision time scale, which provides total energy conservation with relative standard deviation $\delta E/E < 10^{-13}$.

To investigate the effects of contact breaking, we will measure two physical quantities as a function of the amplitude (or temperature) of the thermal fluctuations. We will first study the change in the constant volume specific heat ΔC_V from its zero-temperature value $C_V^0 = 2N'k_b$:

$$\frac{\Delta C_V(T)}{C_V^0} = \frac{C_V(T) - C_V^0}{C_V^0}, \tag{6}$$

where $C_V = dE/dT$ and k_b is the Boltzmann constant. In the low-temperature limit, Eqs. 4 and 5 can be used to calculate the total energy:

$$E = K(t) + \mathcal{U}(t) = \mathcal{U}_0 + \frac{m}{2}\sum_{i=1}^{2N} A_i^2\omega_i^2 = \mathcal{U}_0 + 2N'k_bT, \tag{7}$$

where $\mathcal{U}_0$ is the initial total potential energy. We will measure the specific heat per particle $\overline{C}_V$ in the molecular dynamics simulations by taking the temperature derivative numerically,

$$\overline{C}_V(T) = \frac{1}{N'}\frac{E(T+dT) - E(T)}{dT} = k_b\frac{E(T+dT) - E(T)}{K(T+dT) - K(T)}. \tag{8}$$

From Eq. 8, the deviation in the specific heat per particle can be written as

$$\Delta\overline{C}_V(T)/\overline{C}_V^0 = \frac{1}{2}\frac{E(T+dT) - E(T)}{K(T+dT) - K(T)} - 1. \tag{9}$$

We will also quantify the changes in the average positions of the disks, Δr, as a function of temperature. We define Δr as

$$\Delta r(T) = \sqrt{\frac{1}{N'}\sum_{i=1}^{N'}[(\bar{x}_i(T) - x_i^0)^2 + (\bar{y}_i(T) - y_i^0)^2]}, \tag{10}$$

where (x_i^0, y_i^0) are the x- and y-coordinates of the ith disk in the $T = 0$ MS packing and $(\bar{x}_i(T), \bar{y}_i(T))$ are the time-averaged x- and y-coordinates of disk i at temperature T. $\Delta r(T)$ can be interpreted as the average distance in the $2N'$-dimensional configuration space between the $T = 0$ MS packing and the packing at finite T. Note that rattler disks are not included in the calculations of Δr.

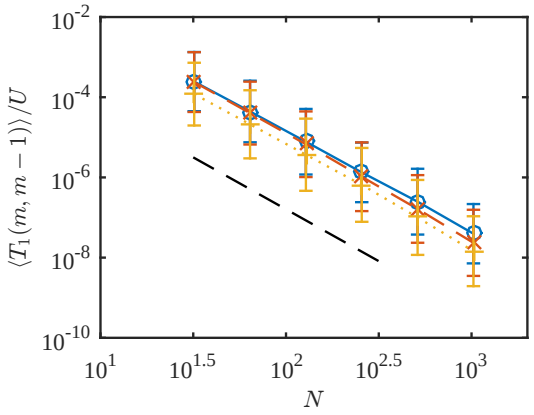

FIG. 3: The minimum temperature $T_1(m, m-1)$ required to break a single contact when perturbing an MS packing along one of the eigenmodes of the dynamical matrix averaged over 5000 MS packings, normalized by the potential energy per particle U, and plotted as a function of system size N. $T_1(m, m-1)$ was obtained by minimizing over all single mode perturbations. We include results for $U = 10^{-12}$ (circles), 10^{-8} (exes), and 10^{-4} (pluses). The slope of the dashed line is -2.6. Rattler disks are removed from the packings prior to performing these calculations.

III. RESULTS

We organize our results into two main sections. In Sec. III A, we discuss the results for the minimum temperatures required to break one or more contacts for single- and multi-mode perturbations. In Sec. III B, we show our results for the temperature dependence of the deviation in the specific heat per particle $\Delta\overline{C}_V$ and deviation in the average disk positions Δr from those in the $T = 0$ MS packing as a function of temperature. For $T < T_{cb}$, form nonlinearities give rise to non-zero values of $\Delta\overline{C}_V$ and Δr. For $T > T_{cb}$, both form and contact-breaking nonlinearities are present. By comparing $\Delta\overline{C}_V$ and Δr for single- and double-sided spring interactions, we can isolate the effects of the contact-breaking nonlin-

earities. We find that for $T_{cb} < T < T_r$ the specific heat deviation $\Delta\overline{C}_V$ scales as N^{-1}, whereas Δr is roughly independent of system size.

A. Temperatures required to break single and multiple contacts

In this section, we study the minimum temperature required to break a given number of contacts in the $T = 0$ MS packing. We first focus on the breaking of a single contact and then study the breaking of multiple contacts. We will show that the temperature required to break the first contact depends strongly on the form of the initial perturbation. For example, the minimum temperature is smaller for perturbations along multiple eigenmodes compared to the minimum temperature for perturbations along a single eigenmode.

At sufficiently low temperatures, we can use the harmonic approximation for the disk positions given in Eq. 5 to calculate exactly the minimum temperature required to break a single contact. If we introduce a perturbation along a single eigenmode k, the minimum temperature required to break a single contact $T_1^k(m, m-1)$ can be calculated by first solving $r_{ij}^2 = \sigma_{ij}^2$ for all contacting disk pairs i and j and then finding the minimum perturbation amplitude (or temperature) over all disk pairs:

$$T_1^k(m,m-1) = \min_{i>j}\left\{\left[\frac{|\vec{\delta}_{ij}^k\cdot\vec{r}_{ij}^0|}{|\vec{\delta}_k^{ij}|^2}\left(\sqrt{1+\frac{(\sigma_{ij}^2-|\vec{r}_{ij}^0|^2)|\vec{\delta}_k^{ij}|^2}{|\vec{\delta}_k^{ij}\cdot\vec{r}_{ij}^0|^2}}-1\right)\right]^2\right\}, \tag{11}$$

where $\vec{\delta}_{ij}^k = \vec{e}_{ij}^k\sin(\omega^k t)/\omega^k$ and $\vec{e}_{ij}^k = (e_{xi}^k - e_{xj}^k, e_{yi}^k - e_{yj}^k)$. To calculate the minimum $T_1^k(m, m-1)$ over all eigenmodes, we set $|\sin(\omega^k t)| = 1$ and find $T_1(m, m-1) = \min_k T_1^k(m, m-1)$. (See additional details in Appendix A.)

In Fig. 3, we show $\langle T_1(m, m-1)\rangle/U$ averaged over 5000 MS packings as a function of system size N for three values of U. We find that $\langle T_1(m, m-1)\rangle$ normalized by U collapses the data and $\langle T_1(m, m-1)\rangle/U$ displays power-law scaling with system-size, $\langle T_1(m, m-1)\rangle/U \sim N^{-\alpha}$, where $\alpha \approx 2.6\pm0.1$. Thus, $\langle T_1(m, m-1)\rangle$ tends to zero in the large system limit [17], which stems from the increasing probability for MS packings to possess anomalously small overlaps as $N \to \infty$.

In several recent publications [27–30], researchers have investigated the stability of zero-temperature packings by measuring the distribution of small interparticle forces using replica symmetry breaking theoretical studies and numerical simulations of frictionless bidisperse disk and sphere packings. The results show that the distribution of force magnitudes $P(F)$ at small forces displays power-law scaling: $P(F) \sim F^\theta$, with an exponent that varies from $\theta \approx 0.2$ to 0.4, depending on the nature of the rearrangement (either local or extended) that results when removing a given small force. (The exponent $\theta \approx 0.2$ is obtained when all small forces are considered.) We measured the minimum interparticle force magnitude, $F_{\min}$, from $P(F)$ as a function of system size N (averaged over an ensemble of 10^3 packings) for repulsive linear spring interactions. We find that the average minimum interparticle force magnitude scales as a power-law with system size, $F_{\min} \sim N^{-\delta}$, where $\delta \sim 0.8$. For repulsive linear springs, the power-law scaling of the minimum overlap with system size is similar $(1 - r_{ij}/\sigma_{ij})_{min} \sim N^{-1}$.

We now consider multi-mode perturbations and measure the minimum temperature required to break a single contact in $T = 0$ MS packings. If we include n eigenmodes in the perturbation, in the low-temperature limit, the disk positions and velocities are given by

$$\vec{V}(t) = \sum_{k=1}^{n} A_k\omega^k\hat{E}^k\cos(\omega^k t), \tag{12}$$

and

$$\vec{R}(t) = \vec{R}^0 + \sum_{k=1}^{n} A_k\hat{E}^k\sin(\omega^k t). \tag{13}$$

As for the single eigenmode perturbations, we can use the harmonic expression for $\vec{R}(t)$ (Eq. 13) to determine the minimum temperature required to break a single contact for multi-mode perturbations. Setting $r_{ij}^2 = \sigma_{ij}^2$ for each pair of disks in the force-bearing backbone yields an expression similar to that in Eq. 11, except $\vec{\delta}_k^{ij}$ is replaced by $\vec{\delta}^{ij} = \sum_{k=1}^n \vec{e}_{ij}^k\sin(\omega^k t)/\omega^k$. The minimum temperature required to break a single contact is obtained by evaluating the extrema of the sine functions, $|\sin(\omega^1 t)| = |\sin(\omega^2 t)| = \ldots = |\sin(\omega^n t)| = 1$, where we must check all combinations of $\sin(\omega^k t) = \pm1$, and by minimizing over all contacting disk pairs. For small n, we discretize all of the possible eigenmode amplitude ratios between 10^{-2} and 10^2 and identify the amplitude ratio combination that yields the minimum temperature $T_n(m, m-1)$ to break a single contact. For $n = 2$ and 3, we explicitly showed that $T_n(m, m-1)$ is minimized (over all possible perturbations) for equal velocity-amplitude perturbations. For $n > 3$, we assumed that $A_1\omega^1 = A_2\omega^2 = \ldots = A_k\omega^k$ perturbations give the minimum $T_n(m, m-1)$. (Additional details concerning these calculations are included in Appendix A.)

In Fig. 4 (a), we plot $T_n(m, m-1)/U$ for single MS packings using multi-mode perturbations as a function of the number of eigenmodes $n = 1, 2, \ldots, 6$ for three values of U, 10^{-12}, 10^{-8}, and 10^{-4}. For all U, we find that $T_n(m, m-1)/U$ decreases with increasing n and then begins to saturate for $n \gtrsim 6$. In general, the minimum temperature required to break a single contact decreases with an increasing number of eigenmodes in the perturbation because the perturbation is more likely to have a significant projection onto the separation vector corresponding to the smallest overlap between disks. Saturation of $T_n(m, m-1)$ with increasing n is interesting

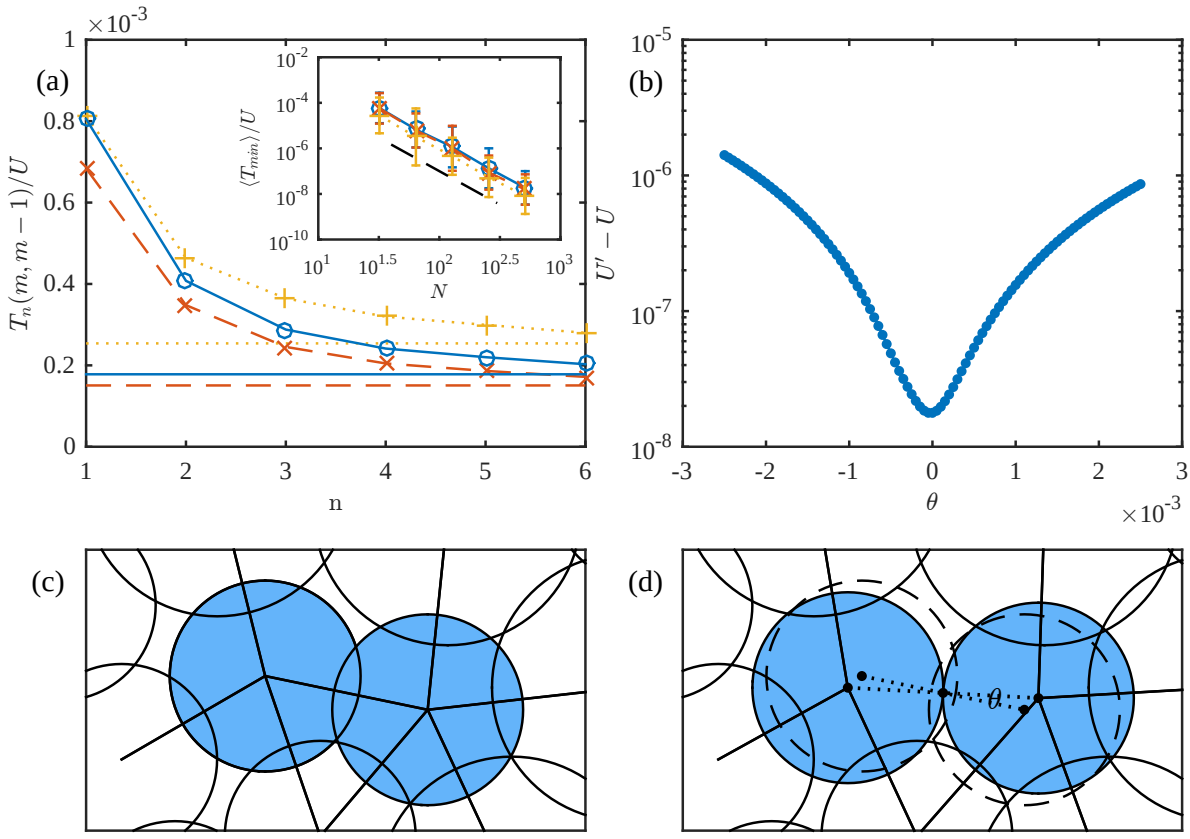

FIG. 4: (a) The minimum temperature $\langle T_n(m,m-1)\rangle$ (normalized by U and averaged over 5000 MS packings) required to break a single contact in response to perturbations that include $n = 1, 2, \ldots, 6$ eigenmodes of the dynamical matrix. $\langle T_n(m,m-1)\rangle$ is obtained by minimizing over all possible n-mode combinations of the $2N'-2$ eigenmodes for each MS packing at $U = 10^{-12}$ (dashed line), 10^{-8} (solid line), and 10^{-4} (dotted line). The horizontal lines give the minimum temperature $\langle T_{min}/U\rangle$ required to remove the smallest overlap between a pair of contacting disks at each U (averaged over 500 MS packings). The inset shows the scaling of $\langle T_{min}/U\rangle$ with system size N for the same values of U as in the main panel. The slope of the dashed line is -2.9. (b) Difference in the potential energy per particle between MS packings before (U) and after (U') separating the pair of disks with the smallest interparticle overlap as a function of the angle θ between the old and new separation vectors between the two disks. (c) and (d) Schematic of the process to measure T_{min}/U. In panel (c), the disk pairs with the smallest overlap are shaded in blue. In panel (d), this pair of disks is shifted so that $r_{ij} = \sigma_{ij}$. The original positions are indicated by the dashed circles. The new separation vector makes an angle θ with the old separation vector (as indicated by the dotted lines). After shifting disks i and j, potential energy minimization is performed allowing all disks to move except i and j. In both panels, the contact networks of the blue-shaded disks are indicated by solid lines.

because it implies that the probability to obtain a pair of disks in the force-bearing backbone with vanishing overlap is zero in any finite-sized system with $U > 0$.

We also developed a method to estimate $T_n(m,m-1)$ in the large-n limit, which is illustrated in Fig. 4 (c) and (d). We first identify the pair of disks i and j in the force-bearing backbone with the smallest overlap. We separate disks i and j so that $r_{ij} = \sigma_{ij}$, while maintaining the center of mass of the two disks and fixing all of the positions of the other disks in the MS packing. We then minimize the total potential energy, allowing all disks to move except disks i and j, as a function of the angle θ between the old and new separation vectors before minimization. In Fig. 4 (b), we plot the difference $U' - U$ in the potential energy per particle before (U) and after (U') shifting disks i and j and minimizing the potential energy as a function of θ. We find that the $\theta = 0$ direction gives rise to the smallest energy barrier, and thus we define the temperature scale $T_{min} = U'(\theta = 0) - U$. T_{min}/U provides an accurate estimate of the large-n plateau value of $T_n(m,m-1)/U$. (See Fig. 4 (a).) In the inset of Fig. 4 (a), we show $\langle T_{min}\rangle/U$ averaged over 500 MS packings as a function of system size. $\langle T_{min}\rangle/U \sim \langle T_n(m,m-1)\rangle/U \sim N^{-\beta}$, where $\beta \approx 2.95 \pm 0.05$, and displays stronger system-size dependence than $\langle T_1(m,m-1)\rangle/U$.

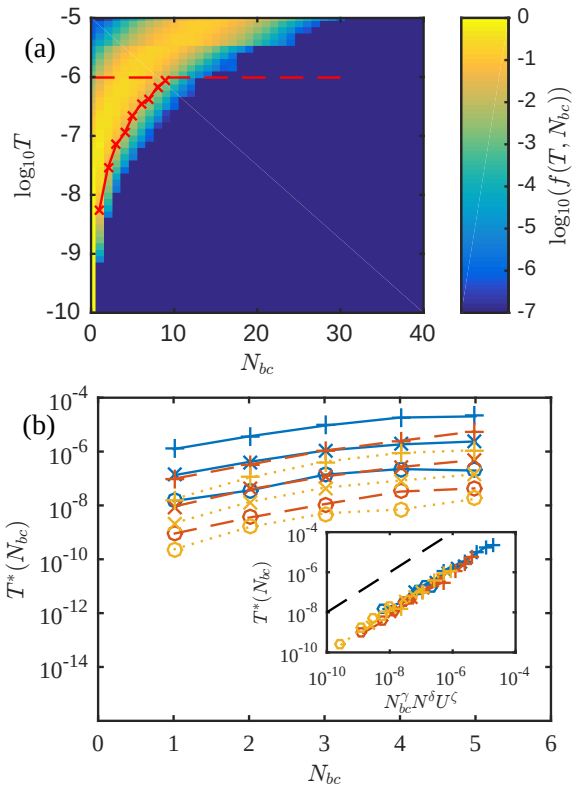

FIG. 5: (a) The fraction of time $f(T, N_{bc})$ that the system (with $N = 64$ and $U = 10^{-4}$) possesses a given number of broken contacts $N_{bc} = N_c^0 + m - N_c$ at temperature T. The color scale from yellow to blue represents decreasing f on a $\log_{10}$ scale. The horizontal line indicates the rearrangement temperature T_r. The solid curve with exes gives the characteristic temperature $T^*(N_{bc}) < T_r$ for multiple contact breaking for which the fraction $f = 0.1$. (b) The characteristic temperature $T^*(N_{bc})$ for three system sizes, $N = 32$ (solid lines), 64 (dashed lines), and 128 (dotted lines), and three values of U, 10^{-5} (circles), 10^{-4} (exes), and 10^{-3} (pluses), for each N. The inset shows the same data as in the main panel, but T^* is plotted as a function of $N_{bc}^{\gamma}N^{\delta}U^{\zeta}$, where $\gamma \approx 2.2 \pm 0.3$, $\delta \approx -2.2 \pm 0.2$, and $\zeta \approx 1.0 \pm 0.1$. The slope of the dashed line is 1.

Thus far, we have focused on the minimum temperature T_{cb} required to break a single contact in $T = 0$ MS packings for different forms of the initial perturbations. For these calculations, we used the harmonic approximation to determine the time-dependent disk positions following the perturbation. We now consider temperatures beyond which multiple $T = 0$ contacts can break and new contacts can form. As discussed previously in Ref. [11, 17], the eigenmodes and associated eigenvectors can change significantly from those at $T = 0$ for $T > T_{cb}$, where new contacts can form and contacts at $T = 0$ can break. Thus, for multiple contact breaking, we use constant energy molecular dynamics simulations to directly measure the number of contacts as a function of time following equal velocity-amplitude perturbations. For these studies, we remove rattler disks prior to starting the simulations and focus on the temperature range $T < T_r$.

During long trajectories, we measure the fraction of time $f(T, N_{bc})$ at each temperature T that the system possesses a given number of broken contacts $N_{bc} = N_c^0 + m - N_c$. We show $f(T, N_{bc})$ for a system with $N = 64$ and $U = 10^{-4}$ in Fig. 5 (a). At low temperatures $T < 10^{-9}$, f is large only for $N_{bc} = 0$. As T increases, more configurations possess an increasing number of broken contacts. We can define a characteristic temperature $T^*(N_{bc})$ for multiple contact breaking by setting $f(T, N_{bc}) = 0.1$.

In Fig. 5 (b), we show the characteristic temperature $T^*(N_{bc})$ for three system sizes N and three values of the initial potential energy per particle, U, for each N. We find that T^* obeys the following scaling form: $T^* \sim N_{bc}^{\gamma}N^{\delta}U^{\zeta}$, where the exponents $\gamma \approx 2.2 \pm 0.3$, $\delta \approx -2.2 \pm 0.2$, and $\zeta \approx 1.0 \pm 0.1$. (Other thresholds $0 < f < 0.1$ give similar values for the exponents γ, δ, and ζ.) The scaling form suggests that $T^*/U \sim N_{bc}^2/N^2 \sim (\Delta m/N)^2$, where Δm is difference in the excess number of contacts at $T = 0$ and finite T^*. This result shows that the temperature required to break an extensive number of contacts scales quadratically with the change in the number of contacts per particle in the range $0 < T < T_r$, which is consistent with prior results [10, 11, 16].

B. Measurement of the deviation of the specific heat and average positions

In this section, we investigate the effects of form and contact-breaking nonlinearities on two physical quantities: 1) the deviation in the specific heat per particle at constant volume, $\Delta\overline{C}_V$, from the value at $T = 0$ and 2) the deviation in the average disk positions Δr from their positions at $T = 0$. We will measure both quantities using constant energy MD simulations with equal velocity-amplitude perturbations involving all eigenmodes (i.e. $A_1\omega^1 = A_2\omega^2 = \ldots = A_k\omega^k$). In general, nonlinearities will cause $\Delta\overline{C}_V > 0$ and $\Delta r > 0$ for temperatures $T > 0$. Form nonlinearities can occur for $T < T_{cb}$, while both form and contact-breaking nonlinearities occur for $T > T_{cb}$.

We show $\Delta\overline{C}_V/\overline{C}_V^0$ (defined in Eq. 9) as a function of temperature T/T_{cb} (normalized by the temperature T_{cb} required to break a single contact) for several system sizes for purely repulsive linear springs ($\alpha = 2$ in Eq. 1) in Fig. 6 (a). For purely repulsive linear springs, the deviation $\Delta\overline{C}_V/\overline{C}_V^0$ is set by the noise floor for $T < T_{cb}$, and thus deviations in the specific heat per particle from form nonlinearities for $T < T_{cb}$ are below the noise floor. In Fig. 6 (b), we compare $\Delta\overline{C}_V/\overline{C}_V^0$ for purely repulsive linear and Hertzian springs ($\alpha = 5/2$ in Eq. 1) as a function of T/T_{cb}. As expected, the form nonlinearities are larger

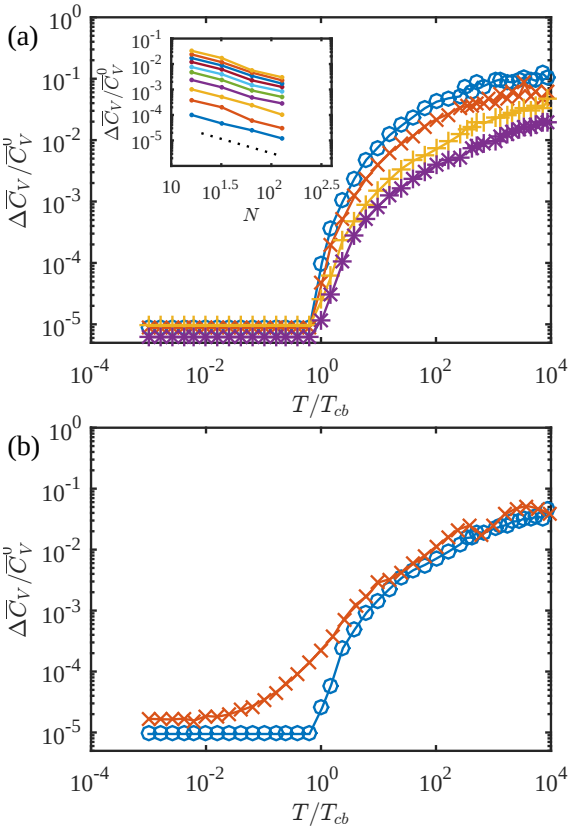

FIG. 6: (a) The normalized deviation in the specific heat per particle at constant volume from the value at $T = 0$, $\Delta\overline{C}_V/\overline{C}_V^0$, at $U = 10^{-5}$ for purely repulsive linear spring interactions as a function of temperature T normalized by T_{cb}, where the first contact breaks. The data is obtained from MD simulations at constant energy following equal velocity-amplitude perturbations applied to 50 $T = 0$ MS packings with $N = 16$ (circles), 32 (exes), 64 (pluses), and 128 (stars). The inset shows $\Delta\overline{C}_V/\overline{C}_V^0$ versus system size N for 10 values of T/T_{cb} from 1 to 10^2 (from bottom to top). The dotted line has slope -1. (b) $\Delta\overline{C}_V/\overline{C}_V^0$ as a function of T/T_{cb} for MS packings with $N = 32$ disks that interact via purely repulsive linear (circles) and Hertzian spring interactions (exes) at $U = 10^{-5}$.

for Hertzian interactions. In particular, the deviation in $\Delta\overline{C}_V/\overline{C}_V^0$ is above the noise floor for $T < T_{cb}$.

For purely repulsive linear springs, $\Delta\overline{C}_V/\overline{C}_V^0$ increases strongly above the noise floor for temperatures near T_{cb}. $\Delta\overline{C}_V/\overline{C}_V^0$ for purely repulsive Hertzian springs also increases rapidly, but the onset of the rapid increase is not as sharp and occurs for $T < T_{cb}$. However, the rate of increase of $\Delta\overline{C}_V/C_V^0$ slows for increasing system sizes. In the inset to Fig. 6 (a), we plot $\Delta\overline{C}_V/\overline{C}_V^0$ for 10 values of T/T_{cb} in the range from 1 to 10^2 as a function of system size for purely repulsive linear springs. We find that the deviation scales as $\Delta\overline{C}_V/\overline{C}_V^0 \sim N^{-1}$ for a wide range of T/T_{cb}, which implies that the effect of both form and contact-breaking nonlinearities on the specific heat vanishes in the large-system limit in this temperature range.

We also study the change in the average disk positions Δr (defined in Eq. 10) as a function of temperature using constant energy MD simulations with equal velocity-amplitude initial perturbations involving all eigenmodes. We consider both purely repulsive (single-sided) and double-sided linear and nonlinear spring interactions. In Figs. 7 (a) and 8, we show $\Delta r^{ds}(T)$ (double-sided) and $\Delta r^{ss}(T)$ (single-sided) for disk packings with $N = 64$, $U = 10^{-5}$, and linear and Hertzian spring interactions. For double-sided linear and Hertzian spring interactions, with no contact breaking, $\Delta r^{ds} \sim T$ over a wide range of T.

This scaling behavior for $\Delta r^{ds}(T)$ stems from form nonlinearities in the total potential energy $\mathcal{U}$, which when expanded gives:

$$\mathcal{U} = \mathcal{U}^0 - \sum_i F_i^0 \Delta R_i + \frac{1}{2!}\sum_{i,j} D_{ij}^0 \Delta R_i \Delta R_j + \frac{1}{3!}\sum_{i,j,k} G_{ijk}^0 \Delta R_i \Delta R_j \Delta R_k + \ldots, \tag{14}$$

where $\Delta\vec{R} = \vec{R} - \vec{R}^0$, $F_i^0 = -\partial V/\partial R_i|_{\Delta\vec{R}=0}$, $D_{ij}^0 = \partial^2 V/(\partial R_i \partial R_j)|_{\Delta\vec{R}=0}$, and $G_{ijk}^0 = \partial^3 V/(\partial R_i \partial R_j \partial R_k)|_{\Delta\vec{R}=0}$. For $T < T_{cb}$, when the contact network does not change, the third-order term in the expansion of $\mathcal{U}$ gives rise to the scaling $\Delta r = CT$, where C is set by G^0. (See Appendix D for the calculation of Δr for a potential with cubic terms in 1D.) Rattler disks are excluded from the measurement of Δr because collisions between backbone and rattler disks will introduce additional nonlinearities. (Δr^{ss} for an MS packing with rattlers is shown in Appendix B.)

As expected, for $T < T_{cb}$, $\Delta r^{ss} = \Delta r^{ds} \sim T$, before contact breaking occurs for both linear and Hertzian spring interactions. The disk displacements in this regime are small and randomly oriented (Fig. 7 (b)). For purely repulsive linear spring interactions in the temperature regime $T > T_{cb}$, Δr^{ss} begins to grow rapidly, reaching values that are several orders of magnitude above Δr^{ds}. In the temperature regime $T_{cb} < T < T_r$, some collective motion occurs and disks can disconnect from the force-bearing backbone and become rattlers (Fig. 7 (c)). At $T = T_r$, Δr^{ss} jumps discontinuously when the system switches to the basin of a new MS packing. (See Appendix C for a discussion of the method that we used to measure T_r.) In the temperature regime $T_r < T < T_g$, strong collective motion can occur and all of the disks can disconnect from the force-bearing backbone when rattler disks are identified recursively (Fig. 7 (d)). Similar behavior occurs for the deviations in the average positions for purely repulsive Hertzian spring interactions (Fig. 8), i.e. Δr^{ss} increases above Δr^{ds} in the temperature regime $T_{cb} < T < T_r$, but the increase is more modest than that for repulsive linear springs. Comparing the disk positions at temperatures $T > T_g$ and zero is not meaningful.

In Fig. 9 (a), we plot the displacement ratio $\Delta r^{ss}/\Delta r^{ds}$

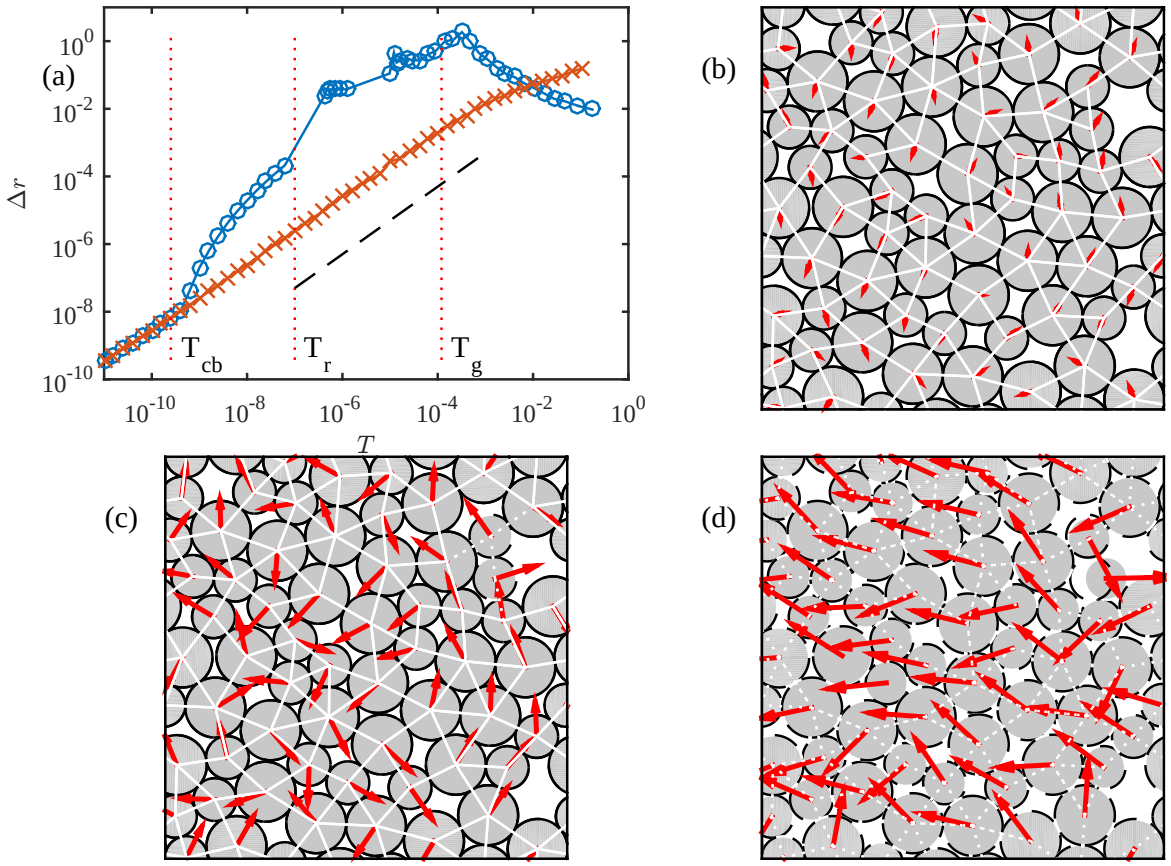

FIG. 7: (a) The deviation Δr in the disk positions from their $T = 0$ values as a function of temperature T for a MS packing with $N = 64$ and $U = 10^{-5}$. The data is obtained from constant energy MD simulations with equal velocity-amplitude initial perturbations involving all eigenmodes. We consider both purely repulsive linear spring interactions (circles; $\alpha = 2$ in Eq. 1) and double-sided linear spring interactions (exes; $\alpha = 2$ in Eq. 2). The dashed line has slope 1. The three dotted vertical lines indicate 1) the measured temperature T_{cb} at which the first contact breaks, 2) the temperature T_r at which the system transitions to the basin of a new MS packing, and 3) the temperature T_g at which the structural relaxation time (from the self part of the intermediate scattering function) appears to diverge. (b) The average disk positions at a temperature $T < T_{cb}$ (gray-shaded disks). White solid lines indicate contacts between disks in the backbone. The arrows represent the displacement of the disks relative to their positions at $T = 0$, where the length of each arrow is proportional to the logarithm of the displacement of the disk . (c) Same as in (b) except for the average disk positions at a temperature $T_{cb} < T < T_r$. Gray-shaded disks without edges are rattlers, circular outlines with dashed edges indicate the initial positions of rattler disks, and white-dotted lines show contacts that include rattlers. (d) Same as (c) except for the average disk positions at a temperature $T_r < T < T_g$.

for single- and double-sided linear spring interactions as a function of T/T_{cb} below T_r for three values of U (10^{-5} (circles), 10^{-4} (exes), and 10^{-3} (pluses)) and $N = 128$. We find that the ratio begins growing for $T > T_{cb}$ reaching an approximate plateau value ≈ 100 that increases weakly with decreasing U. Thus, contact-breaking nonlinearities are much larger than form nonlinearities in the temperature range $T_{cb} < T < T_r$ for linear spring interactions. In Fig. 9 (b), we compare the ratio $\Delta r^{ss}/\Delta r^{ds}$ for linear and Hertzian springs for $T_{cb} < T < T_r$. The contact breaking nonlinearities have a much stronger effect on Δr for linear compared to Hertzian spring interactions. This result likely stems from the fact that form nonlinearities are much weaker for linear spring interactions compared to Hertzian spring interactions. In Fig. 9 (c), we plot $\langle \Delta r^{ss}/\Delta r^{ds} \rangle$ averaged over the temperature range $T_{cb} < T < T_r$ for linear spring interactions as a function of system size N for each U. We find that $\langle \Delta r^{ss}/\Delta r^{ds} \rangle$ shows no sign of decreasing with system size. In Fig. 10, we also show that both Δr^{ss} and Δr^{ds} individually do not depend strongly on system size N (for systems with linear spring interactions). These results emphasize that contact-breaking nonlinearities are dominant for MS packings with purely repulsive linear spring interactions in the temperature regime $T_{cb} < T < T_r$.

For many experimental systems of interest (such as granular materials, foams, and dense colloidal suspensions), in which all of the particles can be visualized and

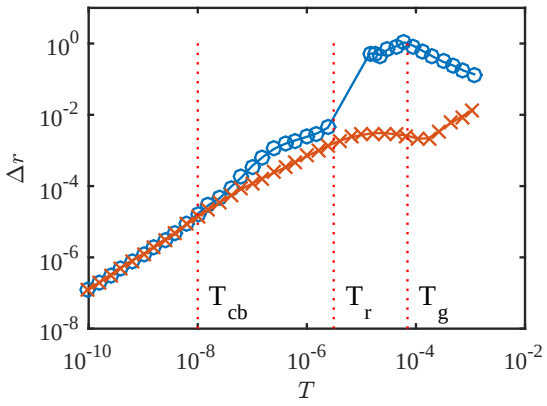

FIG. 8: The deviation Δr in the disk positions from their $T = 0$ values as a function of temperature T for a MS packing with $N = 32$, $U = 10^{-5}$, and single- (circles) and double-sided (exes) Hertzian spring interactions. The three dotted vertical lines indicate T_{cb}, T_r, and T_g (from left to right).

tracked, Δr^{ss} can be measured directly in the experiments. Then, Δr^{ds} can be calculated from numerical simulations using the initial particle positions from experiments. Thus, the ratio $\langle \Delta r^{ss}/\Delta r^{ds} \rangle$ can be measured directly in many experimental systems.

Mechanically stable packings of disks can be represented as local minima in the potential energy landscape (which is a function of all of the positional degrees of freedom in the system). The ratio $\langle \Delta r^{ss}/\Delta r^{ds} \rangle$ tracks the position of the local minimum in the energy landscape as a function of temperature. Thus, by measuring this ratio, we gain insight into the properties of the minima in the energy landscape, which control the thermodynamic properties of granular packings. A number of studies have characterized changes in the local minima in the energy landscape in response to applied shear strain. Here, we show that contact breaking and nonlinearities in the form of the interparticle potential arising from thermal fluctuations can change the position of local minima continuously in the energy landscape.

IV. CONCLUSIONS AND FUTURE DIRECTIONS

In this article, we studied the effects of thermal fluctuations on MS packings composed of bidisperse, frictionless disks generated at different values of the potential energy per particle U or excess number of contacts m/N in two spatial dimensions. We consider disks that interact via single- and double-sided linear and nonlinear spring interactions to disentangle the effects of form and contact-breaking nonlinearities. To identify the temperature range where contact-breaking nonlinearities occur, we first focused on calculating the minimum temperature required to break a single contact in $T = 0$ MS packings for both single- and multi-mode perturbations. Before contact breaking and for weak form nonlinearities (e.g. purely repulsive linear springs), the minimum temperature required to break a single contact can be calculated exactly using the eigenmodes of the dynamical matrix at $T = 0$. Above the contact breaking temperature or for interactions that possess strong form nonlinearities, the eigenvalues and eigenmodes change significantly from those at $T = 0$, and thus the $T = 0$ eigenvalues and eigenmodes cannot be used to calculate the contact breaking temperature accurately.

For single eigenmode perturbations, we find that the minimum temperature (over all single-mode excitations) required to break the first contact, $T_1(m, m-1) \sim U/N^{\alpha}$, where $\alpha \approx 2.6$. This strong system-size dependence emphasizes that weak overlaps between disks in MS packings near jamming onset can break at any finite temperature in the large-system limit. We also showed that the form of the initial perturbation affects the minimum temperature required to break a single contact. The temperature required to break a single contact is minimal for equal velocity-amplitude perturbations involving all eigenmodes of the $T = 0$ dynamical matrix and scales as $T_n(m, m-1) \sim U/N^{\beta}$, where $\beta \sim 2.9$. $T_n(m, m-1)$ can be estimated by identifying the smallest pair of overlapping disks i and j at a given U, shifting them so that their separation satisfies $r_{ij} = \sigma_{ij}$, and then minimizing the potential energy with i and j held fixed, allowing the other disks to move. The difference in the potential energy per particle before (U) and after (U') minimization $U' - U \sim T_n(m, m-1)$ determines the minimum temperature required for breaking a single contact for equal-velocity amplitude perturbations involving all eigenmodes.

Several groups have studied contact breaking in jammed disk and sphere packings undergoing athermal, quasistatic simple shear using computer simulations [31–34]. These studies find that the minimum strain required to break a contact scales as $\gamma_{min} \sim N^{-\lambda}$, where $\lambda = 1$. The system-size scaling exponent λ is smaller than that observed for the minimum temperature required to break a single contact (which is $\approx 2.6 - 2.95$ depending on the form of the initial perturbation). There are several reasons for this difference. First, the previous studies focused on the critical strain amplitude; however, we measured a critical temperature (or energy) scale. Energy and strain are related via $k_bT \sim \gamma^2$, and thus a naive prediction from Refs. [31–34] would be that $T_1(m, m-1) \sim N^{-2}$. However, there is another crucial difference between the two measurements. Contact breaking is determined by the smallest interparticle overlap between a pair of particles, and removing this overlap requires separating these two particles along the line connecting their particle centers. However, the application of athermal, quasistatic simple shear is a perturbation along a single direction in configuration space and there is not necessarily a large overlap between this direction and the direction that separates the smallest interparticle

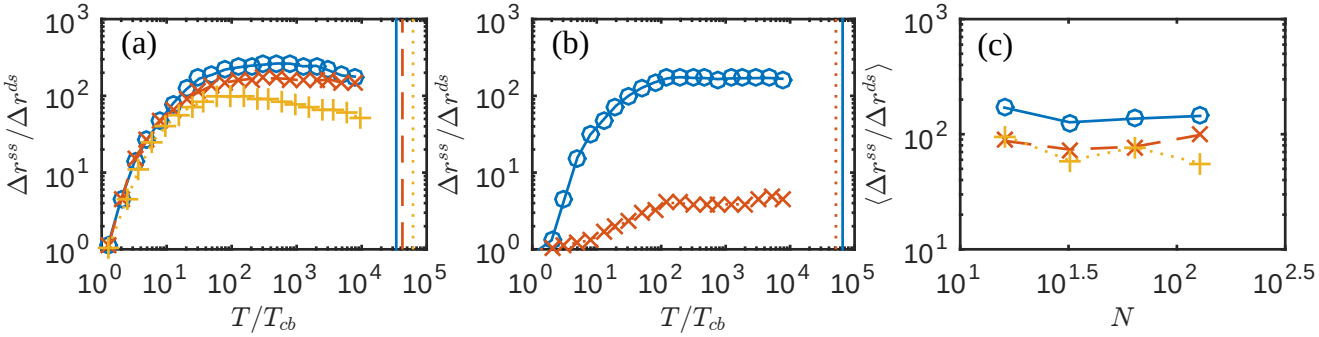

FIG. 9: (a) The ratio $\Delta r^{ss}/\Delta r^{ds}$ between the deviations in positions for single- and double-sided linear spring interactions as a function of temperature normalized by contact-breaking temperature T/T_{cb} for packings with $N = 128$ and three values of U (10^{-5} (circles), 10^{-4} (exes), and 10^{-3} (pluses)). Each curve is averaged over 50 packings in the temperature range $1 < T/T_{cb} < 10^4$. The three vertical lines indicate $\langle T_r \rangle$ for these packings, $U = 10^{-5}$ (solid line), 10^{-4} (dashed line), and 10^{-3} (dotted line). (b) The ratio of position deviations $\Delta r^{ss}/\Delta r^{ds}$ from single- and double-sided linear (circles) and Hertzian (exes) spring interactions as a function of T/T_{cb} for MS packings with $N = 32$ and $U = 10^{-5}$. Each curve is averaged over 50 packings in the temperature range $1 < T/T_{cb} < 10^4$. The two vertical lines indicate $\langle T_r \rangle$ for MS packings with purely repulsive linear (solid line) and Hertzian spring interactions (dotted line). (c) $\langle \Delta r^{ss}/\Delta r^{ds} \rangle$ averaged over the temperature range $1 < T/T_{cb} < 10^4$ for linear spring interactions as a function of system size N for $U = 10^{-5}$ (circles), 10^{-4} (exes), and 10^{-3} (pluses).

overlap. In contrast, thermal fluctuations (which involve all eigenmodes of the dynamical matrix) sample all directions in configuration space. This difference in sampling means that athermal, quasistatic shear perturbations are coupled to the average strain required to break a contact (e.g. where the average is over all eigenmodes). In contrast, thermal perturbations probe the average *minimum* strain (where the minimum is calculated over all eigenmodes for a single packing and then the minimum is averaged over an ensemble of packings). The average *minimum* strain possesses stronger system-size dependence than the average strain.

To study multiple contact breaking, we employed constant energy MD simulations for initial packings at U (and excess number of contacts m) over a range of temperatures $T < T_r$. We measure the fraction of time during the simulations at a given temperature T and system size N that the system possesses $N_{bc} = N_c^0 + m - N_c$ broken contacts. We identify a characteristic temperature $T^*(N_{bc})$ at which a finite fraction f of the time (i.e. $f = 0.1$) the system possesses a given number of broken contacts N_{bc}. By studying a range of U and N, we obtain the following power-law scaling relation: $T^* \sim N_{bc}^{\gamma} N^{\delta} U^{\zeta}$, where $\gamma \approx 2.2 \pm 0.3$, $\delta = -2.2 \pm 0.2$, and $\zeta \approx 1.0 \pm 0.1$. The scaling relation involving integer exponents, $T^*/U \sim (N_{bc}/N)^2$, is within error of the numerical data. These results support prior studies that find that the temperature required to break an extensive number of contacts scales quadratically with the number of contact changes per particle.

We also investigated the effects of form and contact-breaking nonlinearities on the specific heat (at constant volume) and the average disk positions as a function of temperature. We employed both single- and double-sided linear and nonlinear spring interactions, which allowed us to compare the strength of the form and contact-breaking nonlinearities. For the specific heat per particle, we find that the deviation $\Delta \overline{C}_V$ from the zero-temperature value, $\overline{C}_V^0$, is below the noise threshold for $T < T_{cb}$ for purely repulsive linear spring interactions, and begins to increase rapidly for $T > T_{cb}$. For Hertzian interactions, the form nonlinearities give rise to measurable deviations $\overline{C}_V^0/C_V^0$ for $T < T_{cb}$, and the strong increase in $\overline{C}_V^0/C_V^0$ with increasing temperature occurs over a larger range. However, we find that $\Delta \overline{C}_V/\overline{C}_V^0 \sim N^{-1}$ decreases with increasing system size (for purely repulsive spring interactions) in the temperature range $T_{cb} < T < T_r$. Thus, we expect that form and contact-breaking nonlinearities do not have strong effects on the specific heat for $T < T_r$.

We also characterized the change in the average disk positions Δr from their $T = 0$ values arising from form and contact-breaking nonlinearities as a function of temperature. Δr is more sensitive to form and contact-breaking nonlinearities than $\Delta \overline{C}_V$. We first showed that $\Delta r^{ds} \sim T$ for double-sided linear and Hertzian spring interactions over the full range of temperature $0 < T < T_r$ due to form nonlinearities. The linear scaling with temperature arises from third-order terms in the expansion of the total potential energy in terms of the disk positions. As expected, $\Delta r^{ss} = \Delta r^{ds} \sim T$ for $T < T_{cb}$ since there is no contact breaking. Near $T = T_{cb}$, Δr^{ss} begins increasing rapidly above Δr^{ds} for linear springs due to contact-breaking nonlinearities. We show that the ratio $\Delta r^{ss}/\Delta r^{ds}$ can increase by a factor of 100 for $T_{cb} < T < T_r$. In contrast, $\Delta r^{ss}/\Delta r^{ds} < 10$ for Hertzian interactions, presumably because the form nonlinearities are much stronger. We show that $\Delta r^{ss}/\Delta r^{ds}$, Δr^{ss}, and Δr^{ds} (for linear springs) display very weak system size dependence. This result emphasizes that

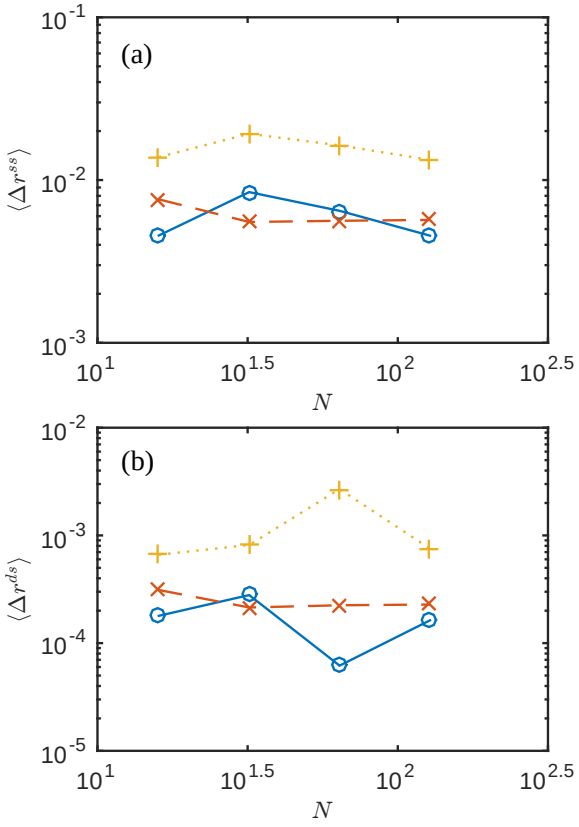

FIG. 10: (a) $\langle \Delta r^{ss} \rangle$ and (b) $\langle \Delta r^{ds} \rangle$ averaged over the temperature range $1 < T/T_{cb} < 10^4$ for linear spring interactions as a function of system size N for $U = 10^{-5}$(circles), 10^{-4} (exes), and 10^{-3} (pluses). Each point is averaged over 50 packings with the same N and U.

contact-breaking nonlinearities are much stronger than form nonlinearities (for linear spring interactions) in this low-temperature regime.

Topics of future studies will include rattler disks, system rearrangements, and nonlinearities induced by non-spherical particle shapes. In most of the current work, we excluded rattler disks by removing them from the MS packing before adding thermal fluctuations. As shown in Appendix B, additional nonlinearities (e.g. collisions between disks in the $T = 0$ force-bearing backbone and rattlers at $T > 0$) are present when rattlers are included in the system. Second, in the current study, we focused on the low-temperature regime $T < T_r$, below which the system remains in the basin of the original $T = 0$ MS packing. In future studies, we will characterize changes in key physical quantities (such as the shear modulus) as the system moves among a series of related basins for $T < T_g$, where the system is prevented from undergoing complete structural relaxation [35]. The current work was important in this context, since we characterized the magnitude of changes in the disk positions that arise from nonlinearities before rearrangements.

At low temperatures $T < T_{cb}$ and for systems with weak nonlinearities, the eigenvalues and associated eigenmodes from the dynamical matrix at $T = 0$ agree with those from $S = \mathcal{V}\mathcal{C}^{-1}$, where $\mathcal{V}_{ij} = \langle v_i v_j \rangle$ is the time-averaged velocity correlation matrix and

$$\mathcal{C}_{ij} = \langle (R_i - R_i^0)(R_j - R_j^0) \rangle \tag{15}$$

is the time-averaged position correlation matrix [11, 36, 37]. An important future direction is to characterize how the eigenmodes of S change as a function of increasing temperature, e.g. do the modes become more or less localized at a given frequency?

Another interesting research direction is to characterize the nonlinearities that arise at finite temperature in MS packings composed of non-spherical particles such as ellipsoids, sphero-cylinders, or other elongated particles. Several studies have shown that packings of ellipsoids possess quartic modes near jamming onset [38–40], i.e. directions along which the potential energy increases as the fourth power of the amplitude in that direction. These results point out that MS packings of non-spherical particles possess form, contact-breaking, and *shape* nonlinearities at finite temperature. Determining the relative strength of these nonlinearities and how they affect the structural and mechanical properties of MS packings at finite temperature is an important, open question.

Acknowledgments

The authors acknowledge financial support NSF grant nos. CMMI-1462439 (C.O. and Q.W.), CMMI-1463455 (M.S.), and CBET-1605178 (C.O. and Q.W.). This work was also supported by the High Performance Computing facilities operated by, and the staff of, the Yale Center for Research Computing.

Appendix A: Calculation of minimum temperature required to break a single contact for equal velocity-amplitude perturbations

In this Appendix, we provide additional details concerning the calculation of the minimum temperature required to break a single contact for perturbations involving multiple $T = 0$ eigenmodes with equal velocity-amplitude excitations. (See Sec. III A.) In Eq. 11, we derived the expression for the minimum temperature required to break a single contact (for $T < T_{cb}$ and systems with weak nonlinearities) by setting $r_{ij}^2 = \sigma_{ij}^2$ and using Eq. 13 for the time-dependent disk positions. Here, we will justify why the the maximum of r_{ij}^2 is obtained when $|\sin(\omega^1 t)| = |\sin(\omega^2 t)| = \ldots = |\sin(\omega^n t)| = 1$, where n is the number of eigenmodes in the initial perturbation. The pair separations satisfy $r_{ij}^2 = x_{ij}^2 + y_{ij}^2$, where

$$x_{ij} = \Delta_x^0 + \sum_{p=1}^{n} \Delta_x^p \sin(\omega^p t) \tag{A1}$$

$$y_{ij} = \Delta_y^0 + \sum_{p=1}^{n} \Delta_y^p \sin(\omega^p t), \tag{A2}$$

the parameters Δ_x^0, Δ_x^1,...,Δ_x^n, and Δ_y^0, Δ_y^1,...,Δ_y^n are constants determined by the initial perturbation and positions of disks i and j. We define $I_{ij}^m = (x_{ij}^m)^2 + (y_{ij}^m)^2$, where $x_{ij}^m = \Delta_x^0 + \sum_{p=1}^m \Delta_x^p \sin(\omega^p t)$, and $y_{ij}^m = \Delta_y^0 + \sum_{p=1}^m \Delta_y^p \sin(\omega^p t)$. When $m = 0$, $I_m = (\Delta_x^0)^2 + (\Delta_y^0)^2$ and when $m = n$, $I_m = r_{ij}^2$. Suppose that when $m = q$, $I_{ij}^q = (x_{ij}^q)^2 + (y_{ij}^q)^2$ is maximal. For $m = q + 1$,

$$I_{ij}^{q+1} = \tag{A3}$$
$$(x_{ij}^q + \Delta_x^{q+1} \sin(\omega^{q+1} t))^2 + (y_{ij}^q + \Delta_y^{q+1} \sin(\omega^{q+1} t))^2.$$

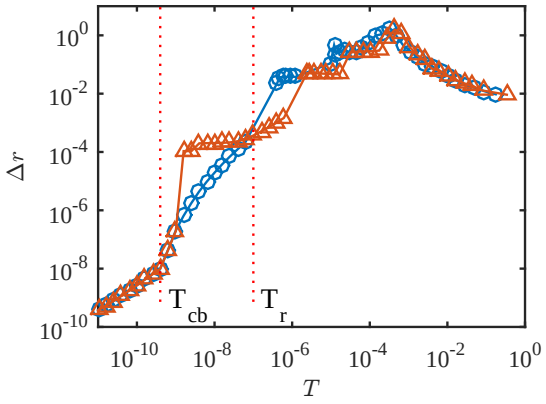

FIG. 11: Δr versus temperature T for an initial MS packing with purely repulsive linear spring interactions, $N = 64$, and $U = 10^{-5}$ with the two rattlers kept in the system (triangles) and the two rattlers removed (circles).

The maximum of I_{ij}^{q+1} is obtained when $dI_{ij}^{q+1}/dt = 0$, which is satisfied when $\cos(\omega^{q+1} t) = 0$ and $|\sin(\omega^{q+1} t)| = 1$. When the proof by induction is repeated, the maximum r_{ij}^2 is obtained if and only if $|\sin(\omega^1 t)| = |\sin(\omega^2 t)| = \ldots = |\sin(\omega^n t)| = 1$. We then study all possible combinations of ± 1 for each of the sine terms and and disk pairs i and j and choose those that give the smallest perturbation temperature.

Appendix B: Measurement of Δr in MS packings with rattlers

In Fig. 7, we showed results for Δr (the deviation of the average positions of the disks from their $T = 0$ values) using constant energy MD simulations as a function of temperature for MS packings with rattlers removed from the system before the perturbations were applied. In this Appendix, we show that rattlers can have a strong effect on Δr by introducing new nonlinearities into the system. In Fig. 11, we compare $\Delta r(T)$ for an MS disk packing with the same force-bearing backbone at $T = 0$ (with purely repulsive linear spring interactions) with and without rattlers removed. (Note that the rattlers do not directly receive thermal excitations.) For sufficiently low temperatures when the rattlers are not excited by fluctuations in the force-bearing backbone, $\Delta r(T)$ is the same for both systems with and without rattlers. For the MS packing studied in Fig. 11, the force-bearing backbone comes into contact with the rattlers at a temperature slightly above T_{cb} (defined using the force-bearing backbone at $T = 0$) and Δr jumps discontinuously for the system with rattlers. (Note that the jump in Δr can occur over a range of temperatures depending on the placement of the rattlers.) Above this temperature, the evolution of Δr is different for the systems with and without rattlers, until the system without rattlers switches to the basin of a new MS packing. Since this article focused on quantifying form and contact-breaking nonlinearities in the temperature regime $T_{cb} < T < T_r$, we mainly performed MD simulations of MS packings with rattlers removed.

Appendix C: Measurement of the rearrangement and glass transition temperatures, T_r and T_g

Our constant energy MD simulations mainly focused on the temperature regime $T_{cb} < T < T_r$, where T_{cb} is the temperature at which the first contact breaks during the simulations and T_r is the temperature below which the system remains in the basin of the $T = 0$ MS packing. To calculate T_r, we first simulate a long trajectory at a temperature T for a given initial perturbation and total time t_{tot}. For each time step of the simulation, we use the current configuration as the initial condition for finding the nearest MS packing (at a given U) using the packing-generation protocol described in Sec. II. We then calculate the fraction f_i of time that the system spends in the basin of MS packing i. The MS packings are distinguished using the eigenvalues of the dynamical matrix.

In Fig. 12, we plot f_i as a function of temperature T after perturbing a given $T = 0$ MS packing with equal velocity-amplitude excitations involving all eigenmodes at each T. We find that three particular MS packings occur most frequently over this range of T and for this initial condition. At the lowest T, only the $T = 0$ MS packing (circles) occurs. At T_r, the fraction of time that the system spends in the $T = 0$ MS packing tends to zero, and the fraction of time that the system spends in a new MS packing (exes) increases to one. At $T \approx 10^{-6}$, the system begins spending time in several MS packings, and at $T \approx 10^{-5}$, the system spends all of its time in a third MS packing (pluses). In most cases, the behavior of $f_i(T)$ mimics that shown in Fig. 12 for the first rearrangement, i.e. there is a rapid drop in occupancy of the $T = 0$ MS packing and a rapid increase in the occupancy of another MS packing at a well-defined temperature. Thus, T_r can be measured accurately for each $T = 0$ MS packing. We

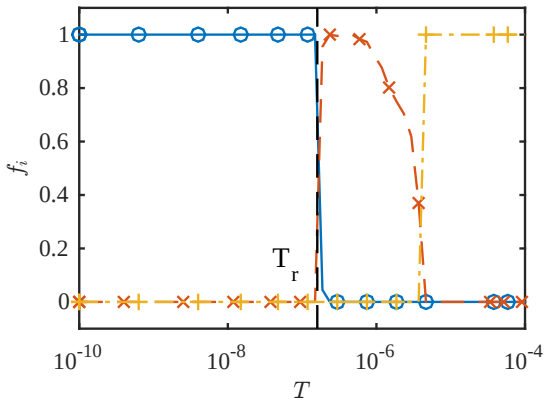

FIG. 12: The fraction f_i of time that three particular MS packings occur in the temperature range $10^{-10} < T < 10^{-4}$ for systems with $N = 64$ and $U = 10^{-5}$. The dashed vertical line indicates the rearrangement temperature T_r for the $T = 0$ MS packing. At the lowest temperatures, the system only populates the $T = 0$ MS packing (circles). At intermediate temperatures a different MS packing (exes) becomes most frequent. At the highest temperatures, the system spends all of the time in a third MS packing (pluses).

also find strong agreement when we measure T_r using f_i and when we define T_r as the temperature at which the first discontinuous jump in Δr occurs for systems where rattlers have been removed. (See Fig. 7 (a).)

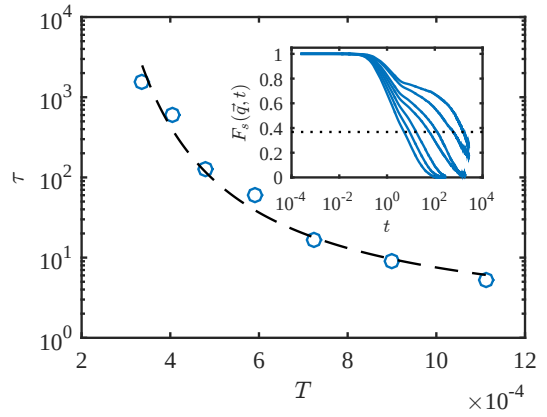

FIG. 13: Structural relaxation time τ (from the decay of the self-part of the intermediate scattering function) as a function of temperature T for a system with $N = 64$ and $U = 10^{-5}$. The dashed line gives $\tau(T) = C \exp[AT_g/(T - T_g)]$, where $C = 1.1$, $A = 15$, and $T_g = 1.3 \times 10^{-4}$. The inset shows the self-part of the intermediate scattering function at $q\sigma_S = 2\pi$, $F_s(q, t)$, for several temperatures from $T = 10^{-4}$ to 10^{-3} from top to bottom. The horizontal line indicates $F_s(q, \tau) = e^{-1}$.

To emphasize that our measurements focus on the extremely low-temperature regime, we also calculated the structural relaxation time from the self-part of the intermediate scattering function (ISF) versus temperature [41]:

$$F_s(\vec{q}, t) = \frac{1}{N} \sum_{j=1}^{N} \langle \exp(-i\vec{q} \cdot [\vec{r}_j(t) - \vec{r}_j(0)]) \rangle, \qquad \text{(C1)}$$

where $\vec{q}$ is the wave number and $\langle \cdot \rangle$ indicates an average over time origins and directions of the wavevector. Near the glass transition temperature, the ISF develops a plateau, whose length increases dramatically with decreasing T. At the longest timescales and for $T > T_g$, the ISF decays as a stretched exponential with stretching exponents that depend on q and T [42]. (See the inset to Fig. 13.) We define a structural relaxation time τ as $F_s(q, \tau) = e^{-1}$ for $q\sigma_S = 2\pi$.

For fragile glasses, the structural relaxation time obeys super-Arrhenius scaling with temperature [43]. As a rough estimate of the glass transition temperature T_g, we use the Vogel-Fulcher-Tammann form [44] for $\tau(T)$:

$$\tau \sim \exp[AT_g/(T - T_g)], \qquad \text{(C2)}$$

where A is a constant and T_g is glass transition temperature at which the structural relaxation time appears to diverge. In Fig. 13, we show that for $N = 64$ and $U = 10^{-5}$, $T_g \approx 10^{-4}$, which is several orders of magnitude larger than T_{cb} and T_r for this system.

Appendix D: The temperature dependence of Δr in model 1D systems

To better understand the temperature scaling of the average position deviation, $\Delta r \sim T$, for MS packings at non-zero temperatures, we studied a model system consisting of a particle in a one-dimensional (1D) potential well. We considered two forms for the potential: a quadratic potential, $U^q(r) = Ar^2/2$, and a cubic potential, $U^c(r) = Ar^2/2 + Br^3/6$ as shown in Fig. 14 (a).

The average position $\langle r \rangle$ as a function of temperature can be calculated using

$$\langle r \rangle = \frac{\int_0^\infty r f(r) dr}{\int_0^\infty f(r) dr}, \qquad \text{(D1)}$$

where the position distribution function in 1D is

$$f(r) = \frac{1}{\sqrt{2(2T - U(r))}}. \qquad \text{(D2)}$$

For the quadratic potential, the average particle position $\langle r \rangle = 0$ for all T. In contrast, for the cubic potential, $|\langle r \rangle| = BT/A^2$ increases linearly with T with a slope that scales with the coefficient of the cubic term. A similar analysis can be applied to MS packings of disks. Before contact breaking, the system lies in a high-dimensional potential energy well. All of the potentials that we studied (i.e. Eqs. 1 and 2 with $\alpha = 2$ and 5/2) possess "form" nonlinearities with nonzero values for the third derivatives of the total potential energy with respect to the

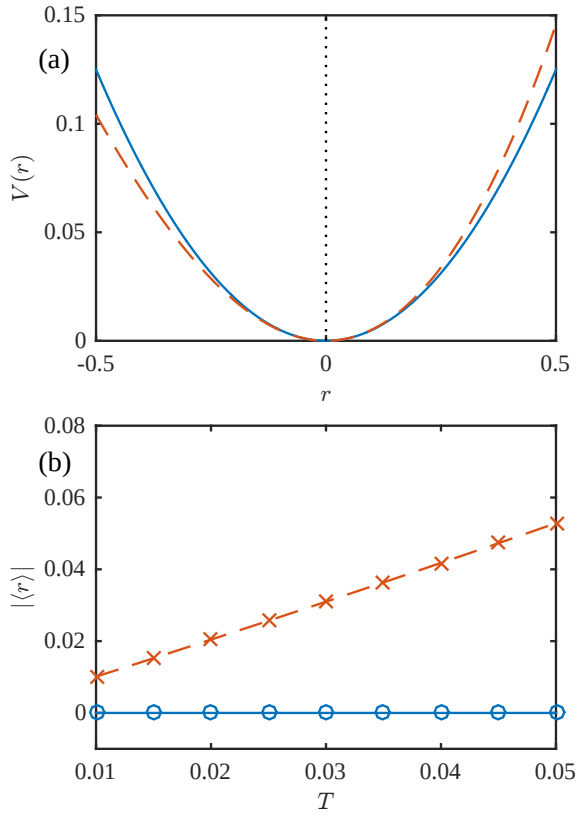

FIG. 14: (a) The potential energy $U(r)$ as a function of position r for a quadratic form, $U^q(r) = Ar^2/2$ (solid line), and a cubic form, $V^c(r) = Ar^2/2 + Br^3/6$ (dashed line). The vertical dotted line indicates $r = 0$. Note that the cubic potential is asymmetric about $r = 0$. (b) The absolute value of the average position $|\langle r \rangle|$ versus temperature T for the quadratic (circles) and cubic (exes) potentials.

disk positions (Eq. 14). Thus, similar to the model 1D system, Δr in MS packings before contact breaking is proportional to the temperature T with a slope that is determined by the third-derivative of the potential energy with respect to the particle coordinates in the direction of the initial perturbation.

[1] H. M. Jaeger, S. R. Nagel, and R. P. Behringer, Rev. Mod. Phys. **68**, 1259 (1996).
[2] G. L. Hunter and E. R. Weeks, Rep. Prog. Phys. **75**, 066501 (2012).
[3] A. V. Tkachenko and T. A. Witten, Phys. Rev. E **60**, 687 (1999).
[4] N. Xu, J. Blawzdziewicz, and C. S. O'Hern, Phys. Rev. E **71**, 061306 (2005).
[5] S. Alexander, Physics reports **296**, 65 (1998).
[6] C. S. O'Hern, L. E. Silbert, A. J. Liu, and S. R. Nagel, Phys. Rev. E **68**, 011306 (2003).
[7] A. J. Liu and S. R. Nagel, Ann. Rev. Condens. Matter Phys. **1**, 347 (2010).
[8] M. van Hecke, J. Phys.: Condens. Matter **22**, 033101 (2009).
[9] A. Ikeda and L. Berthier, Phys. Rev. E **92**, 012309 (2015).
[10] A. Ikeda, L. Berthier, and G. Biroli, J. of Chem. Phys. **138**, 12A507 (2013).
[11] T. Bertrand, C. F. Schreck, C. S. O'Hern, and M. D. Shattuck, Phys. Rev. E **89**, 062203 (2014).
[12] C. P. Goodrich, A. J. Liu, and S. R. Nagel, Phys. Rev. E **90**, 022201 (2014).
[13] C. Brito, O. Dauchot, G. Biroli, and J.-P. Bouchaud, Soft Matter **6**, 3013 (2010).
[14] C. Coulais, R. P. Behringer, and O. Dauchot, Soft Matter **10**, 2013 (1519).
[15] A. Seguin and O. Dauchot, Phys. Rev. Lett. **117**, 228001 (2016).
[16] L. Wang and N. Xu, Soft Matter **9**, 2475 (2013).
[17] C. F. Schreck, T. Bertrand, C. S. O'Hern, and M. D. Shattuck, Phys. Rev. Lett. **107**, 078301 (2011).
[18] S. Atkinson, F. H. Stillinger, and S. Torquato, Proc. Natl. Acad. Sci. U.S.A. **111**, 18436 (2014).
[19] C. P. Goodrich, A. J. Liu, and S. R. Nagel, Phys. Rev. Lett. **109**, 095704 (2012).
[20] Y. Wu, P. Olsson, and S. Teitel, Phys. Rev. E **92**, 052206 (2015).
[21] T. Shen, C. F. Schreck, B. Chakraborty, D. E. Freed, and C. S. O'Hern, Phys. Rev. E **86**, 041303 (2012).

[22] L. Berthier and T. A. Witten, Phys. Rev. E **80**, 021502 (2009).
[23] M. Ozawa, T. Kuroiwa, A. Ikeda, and K. Miyazaki, Phys. Rev. Lett. **109**, 205701 (2012).
[24] C. F. Schreck, C. S. O'Hern, and M. D. Shattuck, Granular Matter **16**, 209 (2014).
[25] C. F. Schreck, C. S. O'Hern, and L. E. Silbert, Physical Review E **84**, 011305 (2011).
[26] S. Warr and J. M. Huntley, Phys. Rev. E **52**, 5596 (1995).
[27] E. Lerner, G. Düring, and M. Wyart, Computer Physics Communications **184**, 628 (2013).
[28] P. Charbonneau, E. I. Corwin, G. Parisi, and F. Zamponi, Physical review letters **109**, 205501 (2012).
[29] E. DeGiuli, E. Lerner, C. Brito, and M. Wyart, Proceedings of the National Academy of Sciences **111**, 17054 (2014).
[30] E. Lerner, G. Düring, and M. Wyart, Soft Matter **9**, 8252 (2013).
[31] J. Boschan, D. Vågberg, E. Somfai, and B. P. Tighe, Soft matter **12**, 5450 (2016).
[32] M. S. van Deen, B. P. Tighe, and M. van Hecke, Physical Review E **94**, 062905 (2016).
[33] M. S. van Deen, J. Simon, Z. Zeravcic, S. Dagois-Bohy, B. P. Tighe, and M. van Hecke, Physical Review E **90**, 020202 (2014).
[34] G. Combe and J.-N. Roux, Physical Review Letters **85**, 3628 (2000).
[35] P. Charbonneau, J. Kurchan, G. Parisi, P. Urbani, and F. Zamponi, Nature Communications **5**, 3725 (2014).
[36] C. Brito and M. Wyart, J. Chem. Phys. **131**, 024504 (2009).
[37] S. Henkes, C. Brito, and O. Dauchot, Soft Matter **8**, 6092 (2012).
[38] C. F. Schreck, M. Mailman, B. Chakraborty, and C. S. O'Hern, Phys. Rev. E **85**, 061305 (2012).
[39] A. Donev, R. Connelly, F. H. Stillinger, and S. Torquato, Phys. Rev. E **75**, 051304 (2007).
[40] Z. Zeravcic, N. Xu, A. J. Liu, S. R. Nagel, and W. van Saarloos, Europhys. Lett. **87**, 26001 (2009).
[41] W. Kob and H. C. Andersen, Phys. Rev. E **52**, 4134 (1995).
[42] G. Wahnström, Phys. Rev. A **44**, 3752 (1991).
[43] C. A. Angell, Science **267**, 1924 (1995).
[44] L. S. Garcia-Colin, L. F. del Castillo, and P. Goldstein, Phys. Rev. B **40**, 7040 (1989).